Tonal Fan Noise Simulation of a V2527 Aircraft Engine: A Quantitative Assessment of a Best Practice Mesh

Carolin Kissner[1], Axel Holewa[1], Sébastien Guérin[1]

[1] German Aerospace Center, Institute of Propulsion Technology, Engine Acoustics Dept., 10623 Berlin, Germany

Email: carolin.kissner@dlr.de, axel.holewa@dlr.de, sebastien.guerin@dlr.de

Introduction

The rotor-stator-interaction noise in the fan stage of an engine is a major contributor to the overall noise level of an aircraft, particularly during approach. It is mainly produced by the interaction of the rotor wakes with the downstream stator rows, namely the fan outlet guide vanes (OGV) and the core inlet guide vanes. Due to its significance, its prediction using high-fidelity computational methods is of interest for the scientific community as well as for engine manufacturers.

However, large tonal fan noise computations - encompassing not only the noise generation mechanism within the fan stage but also the tonal noise propagation within the entire bypass duct as well as its radiation into the free field - can be demanding. The key to successfully performing such a simulation is to find a suitable compromise between accuracy and cost. An important aspect contributing to this compromise is the mesh generation. Too conservative assumptions will result in exceedingly fine meshes. Too coarse meshes lead to inaccurate simulations due to high numerical dissipation and dispersion.

In this paper, the tonal fan noise of a real aircraft engine, i.e. the V2527, is investigated using a best practice mesh generation procedure for setting up the simulation. The aim is to assess the standard technique and to precisely quantify numerical losses in the bypass duct and in the far field computational domains. For this assessment, the authors will rely largely on sound power levels (PWL) determined by a mode matching technique, which decomposes pressure fields into acoustic eigenmodes, in the duct domain and by a Ffowcs Williams-Hawkings (FWH) integral method in the far field domain.

Numerical Setup

The tonal fan noise of the V2527 aircraft engine at approach was simulated using the DLR in-house CFD solver TRACE [1]. The Menter SST $k-\omega$ turbulence model [8] was used and the spatial discretization was done via a MUSCL (Monotonic Upstream Scheme for Conservation Laws) method [7] of second order accuracy based on Fromm's scheme. Furthermore, the Harmonic Balance (HB) technique [3] in combination with the phase-shift boundary condition was applied. The non-linear HB technique solves the unsteady Reynolds Averaged Navier-Stokes (uRANS) equations in the frequency domain instead of the time domain, which is computationally faster as shown by Frey et al. [4] and Holewa et al. [5]. The phase-shift boundary condition allows for the reduction of the computational domain to single-passage rotor, OGV, and engine support stator blocks. Also, thin slices with only two cells in the circumferential direction were needed for the far field blocks. The geometry was simplified to facilitate such a reduced, rotationally symmetric domain; bifurcations in the bypass duct and the drooped-nose inlet were thus neglected. The core flow was also not included in the simulation.

Mesh Generation Procedure

For a finite-volume method as used by TRACE, exact solutions to the integral governing equations are approximated by algebraic expressions over finite volumes (or cells). To calculate flow variables, some terms of the governing equations are expressed as face fluxes and a conservation of these fluxes is enforced across the cell boundaries. Flow variables averaged over the cell volume are typically stored in the cell centroid. The size of a cell, therefore, determines how closely the averaged flow variables at the cell centers match their exact values, particularly in flows changing rapidly in space. The dispersion and dissipation effects of a numerical simulation are therefore directly related to the mesh resolution. In this paper, the focus will be on dissipation effects.

The current technique for the generation of structured meshes for turbomachinery applications is loosely based on the findings of Schnell [9]. He conducted detailed investigations into dissipation and dispersion effects for a two-dimensional test case. He determined that a mesh resolution of 20 to 25 points per wavelength (PPW) resulted in a dissipation rate of 0.5 dB per wavelength perpendicular to the wavefront. However, real fan stage simulations are of a far greater complexity. As opposed to the test case, the Mach number as well as the mesh resolution are far from being constant. An established practice is to aim for at least 40 PPW in all directions. In addition, using a dissipation measure based on a wavelength perpendicular to the wavefront is not practical for a three-dimensional computation, since the wavefront changes depending on the acoustic mode and its position within the duct.

In order to design a suitable mesh for the investigation of tonal fan noise, relevant cut-on modes have to be determined. To find relevant modes that characterize the rotor-stator interaction, the Tyler-Sofrin rule [10] was used: $m = hB + kV$. Here, m denotes the azimuthal mode order and k represents an integer value. The harmonic of the blade passing frequency, which can be determined by multiplying the rotational speed of the rotor

Ω with number of rotor fan blades B ($BPF = \Omega \cdot B$), is described by h. The number of rotor fan blades B is 22 and the number of stator fan blades V is 60 for this configuration. In a next step, it is tested whether relevant azimuthal modes are cut-on in the duct. It was determined that all modes are cut-off at the BPF. The azimuthal mode order $m = -16$ is cut-on at the second harmonic of the BPF ($h = 2$) and the azimuthal mode order $m = 6$ is cut-on at the third harmonic of the BPF ($h = 3$). A positive azimuthal mode order signifies that the mode rotates in the same direction as the rotor and vice versa. For this configuration, the aim of the mesh design was to resolve the 2nd harmonic of the BPF with 40 PPW.

The best practice procedure for generating a mesh that fulfills the above-mentioned constraints works as follows: The wavelength in the axial direction is determined at a position up- and downstream of the fan stage respectively in order to find the maximum cell size in axial direction. The mesh resolution in azimuthal direction is - in this case - set based on aerodynamic considerations, i.e. resolving boundary layers and viscous wakes, rather than acoustical ones since the cut-on, azimuthal modes orders are rather small. In the radial direction, modes tend to be most energetic close to the tip radius, so a clustering of the radial grid points near the tip radius is desirable. The radial grid resolution was chosen to be comparable to similar simulations and to avoid high cell aspect ratios, i.e. cells should have similar side lengths in all directions. As a result, 193 radial grid points were used in the inlet section to resolve 4 and up to 14 radial mode orders at the 2nd and 3rd harmonics of the BPF respectively. 129 radial grid points were used in the bypass duct section to resolve up to 7 radial mode orders at the 3rd harmonic of the BPF. The cells in the far field were designed to have the same size as the cells within the duct in acoustically resolved regions. In regions near the boundaries of the far field, a cell stretching was introduced to suppress reflections due to boundary conditions. The resulting best practice mesh contains about 32.5 million grid points. This meshing approach is standardly utilized. Just recently, Holewa et al. [6] were able to demonstrate that numerical results for such a mesh design correspond well with experimental data.

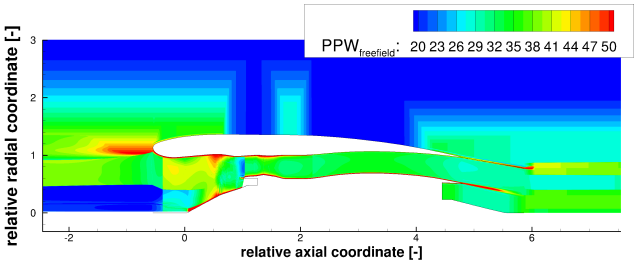

Figure 1: Points per simplified free field wavelength shown for the 2nd harmonic of BPF. PPW was determined for the maximum cell side length at each grid point.

When looking at the resulting mesh in retrospect, it can be seen that the most stringent criterion in terms of cell size stems from the mesh resolution in the far field (see Fig. 1), not from the mesh resolution in the duct. The maximum cell side lengths were determined based on a free field wavelength, which neglects any flow in the far field: $\lambda \approx \frac{c}{f}, \quad \forall\, M \approx 0$. For approach conditions, where the Mach numbers in the free field are small, this simplification is permissible. Since this criterion is more rigorous than any based on acoustic wavelengths in the duct, it would have been a sensible alternative approach to determine a cell size based on far field conditions and keep the cell size constant inside the duct. It would have been a conservative approach based on simplified free field wavelength instead of an approach that requires different considerations for all spatial directions within the duct. This method, however, could only be applied to aircraft engines operating at low rotational speeds and in low free field Mach numbers as is the case during the approach phase.

Duct Analysis

In this section, the sound power within the bypass duct will be analyzed to assess the performance and reliability of the grid. The duct can be subdivided into three distinct sections that will be considered in this investigation: upstream of the fan stage (inlet), downstream of the fan stage (bypass and exhaust), and between fan rotor and stator (interstage). The method used for describing the acoustics inside the duct is an extended triple plane pressure mode matching method as described by Wohlbrandt et al. [11]. This method can distinguish between sound, even discerning between up- and downstream direction of propagation, and convective unsteady pressure fluctuations. However, the method does rely on a few simplifying assumptions: The convective model assumes a uniform mean flow and it neglects any dissipation of the pressure perturbations. In addition, the acoustic model does not consider radial flow but has been extended to solid body swirl.

Figure 2 shows the sound power levels of all acoustic modes at the 2nd and 3rd harmonics of the BPF at different axial positions inside the duct. The dominant sound power levels, that correspond to the main direction of sound propagation, are shown by solid lines. The dotted lines show reflections at the edges of the duct outlet.

Particularly in the domains up- and downstream of the fan stage, the sound power levels of reflections are significantly smaller than prevalent sound power levels, which is to be expected for modes that are well cut-on. The differences are in a range of 10 dB to 35 dB. Furthermore, the main sound power levels decrease nearly linearly with an increasing distance from the fan stage. The dissipation rates in Tab. 1 are given in terms of the decrease in sound power level per stator radius. The dissipation rates up- and downstream of the fan stage are nearly equal for the 2nd harmonic of the BPF. The dissipation rates for the 3rd harmonic of the BPF differ in the up- and downstream domain. They are also higher than for the 1st harmonic. These effects may be attributed to the fact that smaller axial cell sizes are required in the upstream

direction than in the downstream direction, which results in a larger dissipation. The reflections do not show a linear trend. Instead, they are somewhat peaky. This can be explained by the fact that these reflections are much smaller than the dominant sound power levels and their determination may not be as exact.

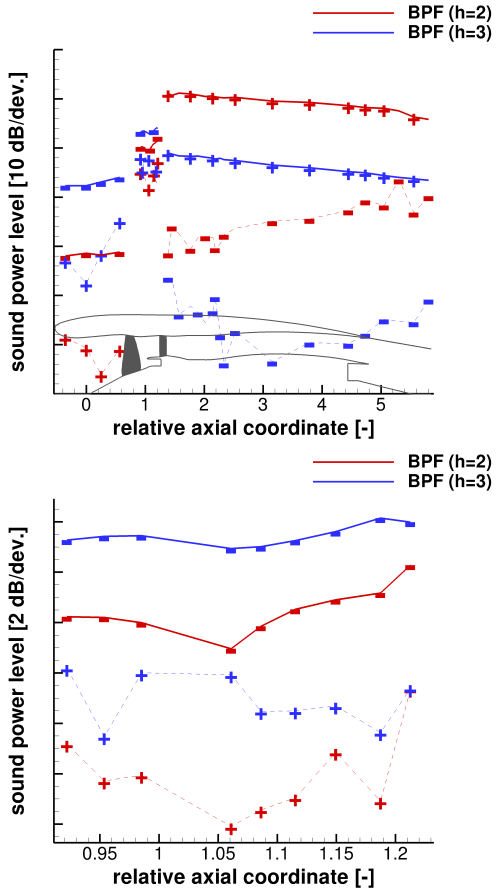

Figure 2: Sound power levels shown for the entire duct (top) and for the interstage section only (bottom). Bold lines: dominant direction of propagation. Dashed lines: reflections. Line symbols (+ or -) indicate the axial propagation direction.

Table 1: Dissipation rates inside the duct up- and downstream of the fan stage. Dissipation rates given as decrease in sound power level per stator radius.

Direction	Harmonic of BPF h	Dissipation Rate [dB/R]
upstream	2	0.7
upstream	3	1.9
downstream	2	0.8
downstream	3	1.2

The dominant direction in the interstage area is the upstream direction. The corresponding sound power levels are nearly constant. Small differences may be caused by the more complex flow in the interstage, which makes the sound power levels more difficult to predict with the used pressure mode matching technique. While the sound is stronger in the upstream direction in the interstage area, the sound power levels are much lower upstream than downstream of the fan stage. The interstage sound power levels decrease significantly as they pass through the rotor. The decrease in sound power for the 2nd harmonic of the BPF is greater than for the 3rd harmonic of the BPF by more than 10 dB. Two factors can contribute to such a shielding effect: Firstly, the swirl in the flow increases the tendency of an acoustic mode to become cut-off if the swirl Mach number and the circumferential mode face in the same direction as is the case for azimuthal mode order 6 at the 3rd harmonic of the BPF. Secondly, azimuthal modes that have the same rotational direction as the rotor are transmitted more effectively. This would explain why the shielding of mode -16 at the 2nd harmonic of the BPF is higher as for mode 6 at the 3rd harmonic of the BPF. The sound power levels seem to indicate that the latter effect is stronger.

Free Field Analysis

To analyze the quality of the mesh in the far field, the sound power was determined using the FWH integral method. The observer positions were placed in a semicircle of radius 100 m around the sound source. While the observer positions remained the same, different integration surfaces were defined up- and downstream of the engine. In theory, the sound power levels should remain constant regardless of the location of the integration surfaces provided the mean flow is uniform and the surface is closed and completely surrounds the source. In practice, numerical dissipation due to the nature of the grid applies too.

The used integration surfaces along with their respective sound power levels are shown in Fig. 3. Whereas all contours show fluctuating pressure levels, note that the scaling varies.

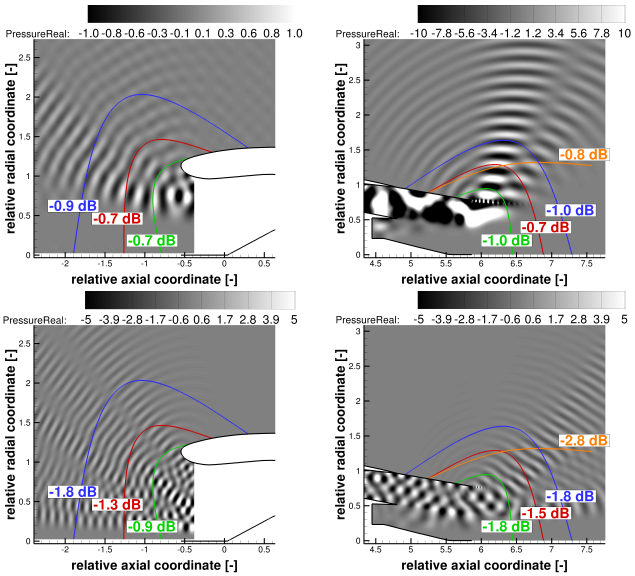

Figure 3: Far field integration surfaces along with their corresponding PWL's (relative to the respective duct PWL's) up- and downstream of the engine for 2nd (top) and 3rd (bottom) harmonics of the BPF. Contours show fluctuating pressure levels.

In the far field upstream of the engine, only integration surfaces fully enclosing the inlet were used. The differences in power between the closest duct position and the integration surfaces is of an expected magnitude given the previously determined dissipation rates within the duct. The sound power obtained at the different integration surfaces show almost no dissipation at the 2nd harmonic of the BPF but some dissipation at the 3rd harmonic of the BPF. This is to be expected since the mesh does not fully resolve the 3rd harmonic.

Downstream of the engine, three closed integration surfaces and an open integration surface were defined. Again, the difference in sound power between the surfaces and the closest position within the duct is to be expected due to the previously determined numerical dissipation and is of a similar magnitude as upstream of the engine. Interestingly, the difference in sound power is nearly the same for the closed and open integration surfaces indicating that the open integration surfaces managed to enclose most of the radiated sound. There is, however, not a clear dissipation trend downstream of the engine. Two other factors make the prediction of sound power more difficult downstream compared to upstream of the engine: Firstly, the FWH integral method assumes a uniform flow and so does the pressure mode matching technique used inside the duct. This assumption does especially not hold true in the presence of shear layers. In Fig. 4, the axial velocity is shown to illustrate the non-uniform flow inside the rear portion of the duct and at the position of the integration surfaces. Secondly, acoustic energy can be converted into vortical energy in the shear layer as has been shown by Berchert [2].

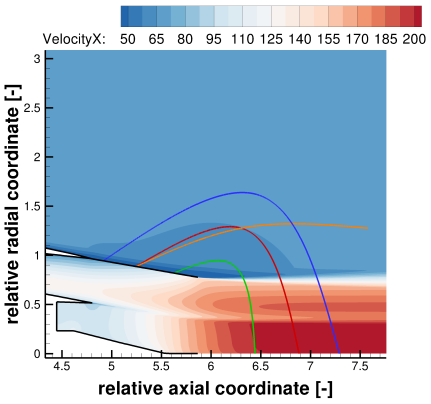

Figure 4: Axial velocity downstream of fan stage.

Conclusion

In this paper, it was demonstrated that a full-scale aircraft engine like the V2527 can be computed efficiently by using the HB method while also yielding reasonable results. The HB simulation ran for approximately 10 days on 120 cores and the obtained results will henceforth be compared to experimental data. The specific aim of this paper was to look critically at the current best practice meshing to assess and possibly improve it in the future.

Using sound power levels in the duct and in the far field allowed for an assessment of the grid quality in terms of numerical dissipation. In the duct, the sound power decreases linearly relative to the distance from the fan stage. The dissipation rates were calculated in terms of a decrease in sound power per stator radius in axial direction instead of per wavelength perpendicular to the wavefront. The used measure is more practical for the simulation of tonal fan noise due to the complex geometry of real aeroengines and the multitude of acoustic modes that need to be considered for such a configuration. The thusly determined dissipation rates have the potential to be used for the correction of numerical data in order to allow for a better comparison with experimental data. They can also be used as a reference for the mesh design of future simulations.

References

[1] Becker, K. et. al.: Recent Progress in a Hybrid Grid CFD Solver for Turbomachinery Flows. ECCOMAS CFD (2010)

[2] Berchert, D.: Sound absorption caused by vorticity shedding, demonstrated with a jet flow. J Sound Vib (1980), 70(3):389-405

[3] Frey, C. et. al.: A Harmonic Balance Technique for Multistage Turbomachinery Applications. ASME Turbo Expo (2014)

[4] Frey, C. et. al.: Simulations of Unsteady Blade Row Interactions using Linear and Non-linear Frequency Domain Methods. ASME Turbo Expo (2015)

[5] Holewa, A. et. al.: CFD-based investigation of turbine tonal noise induced by steady hot streaks. 11th European Conference on Turbomachinery Fluid Dynamics and Thermodynamics (2015)

[6] Holewa, A. et. al.: Tones from an Aero-Engine Fan: Comparison between Harmonic-Balance Simulation and Experiment. 22nd AIAA/CEAS Aeroacoustics Conference (2016)

[7] Lien, F.S. and Leschziner, M.A.: Upstream monotonic interpolation for scalar transport with application to complex turbulent flows. Int J Numer Meth Fl (1994), 19:527-548

[8] Menter, F. R.: Tones from an Aero-Engine Fan: Two-equation eddy-viscosity turbulence models for engineering applications. AIAA/CEAS Journal (1994), 62(3):1598-1605

[9] Schnell, R.: Numerische Simulation des akustischen Nahfeldes einer Triebwerksgebläsestufe. PhD Thesis at TU Berlin (2004)

[10] Tyler, J. M. and Sofrin, T. G.: Axial flow compressor noise studies. SAE Transactions (1962), 70:355-375

[11] Wohlbrandt, A. et al.: A robust extension to the triple plane pressure mode matching method by filtering convective perturbations. Int J Aeroacoust (2016), 15(1-2):41-58